THE JOURNAL OF COMPARATIVE NEUROLOGY 481:194–209 (2005)

Morphological Identification of Ganglion Cells Expressing the α Subunit of Type II Calmodulin-Dependent Protein Kinase in the Macaque Retina

DAVID J. CALKINS,[1,2]* REBECCA M. SAPPINGTON,[1,2] AND STEWART H.C. HENDRY[3,4]

[1]Department of Ophthalmology, The University of Rochester Medical Center, Rochester, New York 14642

[2]The Center for Visual Science, The University of Rochester Medical Center, Rochester, New York 14642

[3]Krieger Mind-Brain Institute, The Johns Hopkins University, Baltimore, Maryland 21218

[4]Department of Neuroscience, The Johns Hopkins University, Baltimore, Maryland 21218

ABSTRACT

Expression of the α subunit of type II calmodulin-dependent protein kinase (αCamKII) distinguishes the koniocellular neurons of the primate lateral geniculate nucleus (LGN) from the primary parvo- and magnocellular neurons, but whether the same neurochemical signature distinguishes the retinal ganglion cells providing them input is not known. We find that, in the retina, αCamKII expression also differentiates two primary groups of ganglion cell, both characterized by broad, sparsely branching dendritic trees and cell bodies intermediate in size between the parvo- and magnocellular-projecting ganglion cells. Cells in the first group have three or four primary dendrites, a thick axon, and a rounded cell body and likely are made up of multiple types. In contrast, ganglion cells in the second group demonstrate a highly regular morphology, with strictly two primary dendrites and a thinner axon emanating from a smaller, elliptical cell body. This cell resembles the "large sparse" ganglion cell identified by others in retrograde labeling from the LGN and represents about 2% of all ganglion cells. In the optic nerve, αCamKII+ axons are also intermediate in size and form a bimodal distribution, correlating with the axonal sizes of the two groups of ganglion cell. For the LGN, we describe a group of αCamKII+ axon terminals with morphology consistent with terminals from retinal ganglion cells. These terminals form long, filamentous contacts with αCamKII+ relay cells and increase in frequency from the dorsal to the ventral koniocellular regions. Our results indicate that ganglion cells expressing αCamKII represent multiple projections to the brain, at least one of which provides input to one or more koniocellular regions of the LGN. J. Comp. Neurol. 481:194–209, 2005.

Indexing terms: ***Macaca fascicularis*** **and** ***mulatta*****; optic nerve; thalamus; calmodulin-dependent protein kinase**

For decades, the primate visual system was thought to begin with only two primary retinal ganglion cell pathways to the lateral geniculate nucleus (LGN) of the thalamus (for review see Kaplan et al., 1990; Schiller and Logothetis, 1990). These two pathways in concert were to encode most aspects of visual information. This bipartite construct arose in part from the observation that the LGN itself contains two primary populations of cortical relay neurons that are anatomically segregated between four dorsal and two ventral layers. Neurons of the dorsal layers are termed "parvocellular" (or P) because of their small cell bodies, whereas neurons of the ventral layers are termed "magnocellular" (or M) because of their greater size. The P cell demonstrates poor contrast sensitivity, a sustained response to light, and a narrow receptive field owing to its input from the small and numerous "midget"

Grant sponsor: National Institutes of Health; Grant number: EY12480 (to D.J.C.); Grant number: EY06432 (to S.H.C.H.); Grant number: EY07125-14 (to R.M.S.); Grant sponsor: Sloan Foundation (to D.J.C.); Grant sponsor: Research to Prevent Blindness, Inc. (to D.J.C.).

*Correspondence to: David J. Calkins, Department of Ophthalmology and Visual Sciences, Vanderbilt University Medical Center, 1401 21st Avenue South, Nashville, TN 37205. E-mail: david.j.calkins@vanderbilt.edu

Received 3 June 2004; Revised 3 August 2004; Accepted 21 September 2004

DOI 10.1002/cne.20368

Published online in Wiley InterScience (www.interscience.wiley.com).

ganglion cell of the retina. The M cell demonstrates higher contrast sensitivity, a transient response, and broader receptive field; it derives retinal input from the larger and more sensitive "parasol" ganglion cell. Because its small receptive field not only is finely tuned spatially but is often spectrally opponent, the P/midget cell is thought to underlie both spatial acuity and color discrimination. Because of its transient response to light, the M/parasol cell encodes temporal signals that are likely to support the discrimination of motion.

This simple model in which information from the retina is parceled between the P and the M pathways is consistent with emerging views of two divergent ventral and dorsal streams in the visual cortices (DeYoe and Van Essen, 1988; Felleman and Van Essen, 1991). However, from the standpoint of optimizing signaling capacity, maximizing sensitivity, and minimizing noise, one might expect the visual system to evolve multiple, specialized retinogeniculate pathways, each tuned to a specific aspect of the visual scene (Sterling, 1998; Calkins and Sterling, 1999). Such specialization would require not two, but many, physiologically distinct pathways. This idea is supported by recent anatomical studies establishing that both the human retina and the retina of nonhuman primates contain a greater diversity of ganglion cell types than generally considered from a historical standpoint (Kolb et al., 1992; Peterson and Dacey, 1999, 2000). Similarly, recent retrograde labeling studies have demonstrated that many of these additional ganglion cell types project to the LGN (Rodieck and Watanabe, 1993; Dacey et al., 2003) and also demonstrate a rich variety of physiologies (Dacey et al., 2003). Finally, a third population of LGN relay neurons is distinguished from the P and M cells by their select expression of certain neurochemical markers, in particular the α subunit of type II calmodulin-dependent protein kinase (αCamKII). These neurons delineate six distinct koniocellular (or K) bands throughout much of the primate LGN, each ventral to a primary P or M layer, but also intersperse sporadically within the primary layers (Casagrande, 1994; Hendry and Yoshioka, 1994; Goodchild and Martin, 1997; Hendry and Calkins, 1998). There is now ample evidence that the small-bistratified ganglion cell implicated in blue/yellow color discrimination projects to one or more K layers within the parvocellular portion of the LGN (Martin et al., 1997; Solomon et al., 2001; White et al., 2001; Chatterjee and Callaway, 2002; Dacey et al., 2003). However, the majority of αCamKII+ neurons are distributed densely in the two K layers embedded in the magnocellular portion of the LGN (K1 and K2), so the blue/yellow cells can represent only a subset of the K pathways (for review see Hendry and Reid, 2000).

A key step in understanding the functional significance of the diversity emerging from these recent studies is establishing whether the various ganglion cell morphologies correlate with a particular neurochemical signature and whether this signature can be linked to a pattern of projection to the LGN or, for that matter, other central retinorecipient structures, such as the superior colliculus or pretectum (see, e.g., Benson et al., 1991). In this study, we demonstrate that expression of αCamKII distinguishes a population of retinal ganglion cells likely belonging to a subset of the wide-field or diffuse ganglion cells described in other studies of the human and macaque retina (Peterson and Dacey, 1999, 2000; Dacey et al., 2003). This αCamKII+ population comprises two primary groups of cells, both with sparsely branching, broad dendritic trees and cell bodies intermediate in size between the larger M and smaller P projecting ganglion cells. The two groups are distinguished by dendritic morphology, somal shape, and axon diameter. A particular group with highly regular morphology demonstrates an elliptical cell body and closely resembles the sparsely-branching diffuse cell described for the human retina (Peterson and Dacey, 2000) and the "large sparse" cell described from retrograde labeling of ganglion cells from the LGN in macaque (Dacey et al., 2003). In the optic nerve, αCamKII+ axons are also intermediate in size and form a bimodal distribution, suggestive of two main groups of ganglion cells. Quantitative analysis indicates that αCamKII+ ganglion cells in total account for about 15% of all ganglion cells, with the elliptical ganglion cell representing about 2%. Finally, our observations extend to the LGN, where we find that αCamKII expression not only delineates the K layers themselves, but also a population of axon terminals whose morphology matches that of retinal terminals. Some of these are presynaptic to αCamKII+ koniocellular neurons, primarily in K1 and K2.

MATERIALS AND METHODS

Animals and tissue preparation

We harvested tissue for these studies from a total of five adult monkeys (*Macaca fascicularis* and *M. mulatta*), adhering strictly to protocols approved by our institutions' animal care and use committees and conforming to the National Institutes of Health guidelines for use of vertebrate animals. After euthanasia with an intravenous overdose of Nembutal (100 mg/kg of body weight), the animals were perfused transcardially with 4% paraformaldehyde and 0.1–0.5% glutaraldehyde in 0.1 M phosphate buffer and the eyes and brain removed. The isolated eyecups were cleaned of vitreous, and the LGN was removed from the brain following 2–3 hours of additional fixation freely floating in the same fixative; both were rinsed repeatedly in 0.1 M phosphate buffer (pH 7.4). Retinas were isolated from the eyecups, freed of choroid and pigment epithelium, and cut into quadrants for use in whole-mount preparations.

Retinal whole-mount immunocytochemistry

For our whole-mount studies (see Figs. 1–6), the retina from an eye of each of three animals was divided into quadrants (temporal superior/inferior and nasal superior/inferior) along the horizontal and vertical meridians through the optic nerve head. Individual quadrants were cryoprotected in graded sucrose solutions (30–10%) and freeze-thawed repeatedly on pieces of dry ice to enhance penetration of the primary antibody. The quadrants were incubated in a blocking solution of 0.8% bovine serum albumin (BSA), 0.1% gelatin, 0.1% Triton X-100, and 5% normal horse serum (NHS) in 0.01 M phosphate-buffered saline (PBS) for 1–2 hours at room temperature. After light rinsing in PBS, the quadrants were transferred into a primary antibody solution of 0.8% BSA, 0.1% gelatin, 1% NHS, and mouse monoclonal antibody against αCamKII (1:2,000 dilution; Boehringer Mannheim Biochima, Indianapolis, IN) in PBS for 2–3 days at 4°C. After rinsing repeatedly in PBS, the quadrants were incubated for 2 hours at room temperature with biotinylated, anti-mouse

secondary antibody (1:200; Vector Laboratories, Burlingame, CA). After PBS rinsing, the quadrants were incubated in Extravidin (1:300; Sigma) for 1.5–2 hours in the dark at room temperature, rinsed, and transferred to Tris buffer. After conjugation with 3,3′-diaminobenzidine (DAB), the quadrants were rinsed and postfixed in 2% glutaraldehyde in cacodylate buffer for 1–2 hours. The quadrants were then mounted on glass slides and coverslipped for light microscopy.

Retinal semithin sections

A small piece of temporal retina 2–3 mm inferior to the fovea was excised from a single quadrant that had been processed for αCamKII labeling as described above and embedded in Epon-Araldite at 60°C for 48 hours. Horizontal semithin sections (1–2 μm thick) were cut from this piece, collected serially on glass slides, and counterstained with toluidene to compare the area of the cell body for stained and unstained ganglion cells (see, e.g., Fig. 2).

Light microscopy and quantification

All light microscopy was performed with an Olympus Provis AX70 upright microscope equipped with a motorized stage and color CCD camera interfaced with a personal computer. Measurements of cell body area and aspect ratio and of axonal area and diameter were obtained by using the trace function of ImagePro (Media Cybernetics). For measuring cell body area in horizontal semithin sections (see Fig. 2), serial sections were imaged, and the greatest cross-sectional area through each cell body was calculated (see Fig. 3). For measurements from the whole-mount preparations (see Figs. 4, 5), the cross-sectional area was obtained by focusing through each cell body and measuring at its greatest diameter (see Fig. 6). Reconstructions of ganglion cells (see Fig. 7A) were computed from stacks of images obtained with differential interface contrast optics in whole-mount preparations by using the 3DReconstructor module of ImagePro. Stratification depth of dendritic trees (see Fig. 7B,C) was measured in whole-mount preparations by recording the distance in Z-axis focus between the cell body in the ganglion cell layer (0% depth) and the most distal visible dendrites as they coursed toward the border of the inner nuclear layer (100% depth). Axon diameter (see Fig. 7D) was measured at its thickest point near the cell body, and aspect ratio was measured at the point of largest diameter (see, e.g., Fig. 8). All measurements were obtained with ×60–100 oil-immersion differential interference contrast objectives with an additional magnification factor of ×2–3 through the computer-CCD camera interface.

Optic nerve and LGN

After euthanasia of two animals, samples of optic nerve 5–6 mm proximal to the eyecup were embedded in agarose, and 40–60-μm-thick vertical sections were cut on a vibratome for preembedding immunocytochemistry for αCamKII (see Figs. 9, 10). Our protocol was similar to that described above for the retinal whole-mount preparations, with the following modifications. Triton X-100 was omitted in the blocking step; the incubation with primary antibody was extended to 3–5 days at 4°C; and, after conjugation of the αCamKII label with DAB, the sections were fixed for 45 minutes in 2% glutaraldehyde in cacodylate buffer and rinsed in cacodylate overnight at 4°C. The sections were postfixed in 1% osmium in cacodylate buffer for 1 hour, rinsed again in cacodylate overnight, dehydrated in graded alcohols, and embedded in Epon-Araldite at 60°C for 48 hours. Ultrathin sections were cut at 70 nm and photographed under a Hitachi 7100 electron microscope at magnifications of ×7,000–30,000. For quantification, we digitized the electron micrographs and applied the trace tool of ImagePro (see above) to measure the contiguous area of cytosol contained within each axon (see Fig. 11). We did not use axonal diameter as a measure of size, to avoid artifacts resulting from poor preservation of myelin or misshapen axons. For electron microscopy of LGN (see Figs. 12–14), blocks of LGN from three animals were cut in the frontal plane on a vibratome at a thickness of 40–60 μm. The protocol was identical to that used for optic nerve. After Epon-Araldite embedding, small pieces of individual sections that contained a high degree of αCamKII immunoreactivity were isolated with a razor blade and used for ultrathin sectioning.

RESULTS

αCamKII+ retinal ganglion cell bodies are intermediate in size

In whole-mount preparations of the retina, αCamKII immunoreactivity clearly distinguishes a population of ganglion cells with finely articulated, broad dendritic trees that often span distances of 150–200 μm in the retinal periphery (Fig. 1). For most cells with such well-labeled dendrites, we were able to identify also a thickly labeled axon. A dense population of amacrine cells, both displaced to the ganglion cell layer and in the inner nuclear layer, also expresses αCamKII. These cells generally lack stained processes, have somas that are far smaller than those of the labeled ganglion cells (about 50% as large), have a prominent nucleus that fills the cell body, and lack an axon altogether. Some small ganglion cells, discriminated from the amacrine cells by the presence of a well-defined nucleus, also express αCamKII, but they only rarely demonstrated labeled dendritic trees and axons (Fig. 1).

In some whole-mount preparations, background staining faintly outlines the somas of other ganglion cells, both the largest (presumably parasol) and the far more numerous smallest (presumably midget) cells. In these cases, the somas of the most intensely stained αCamKII+ ganglion cells appear clearly intermediate in size. However, to illustrate and quantify these differences better, we prepared horizontal sections through a portion of perifovea that had been immunolabeled for αCamKII (Fig. 2). From these sections, we measured somal area for equally sized samples of labeled and unlabeled ganglion cells (Fig. 3). The area of unlabeled cells spans a considerable range, 70–600 μm^2, whereas the range for αCamKII+ cells is only about half as large: 75–360 μm^2. Similarly, the 99% confidence interval for labeled ganglion cells is far narrower than that for unlabeled cells: 187–229 vs. 193–265 μm^2, respectively. This difference is reflected in the median values. Even though the mean for the αCamKII+ cells (207.5 μm^2) is less than the mean for unlabeled cells (229.1 μm^2; see Fig. 3 legend), the median value for labeled cells is higher and shifted toward the middle of the range: 210 μm^2 vs. 188 μm^2 for unlabeled cells.

Perhaps the most notable attribute of the histogram of somal areas in Figure 3 is the peak of the distribution for

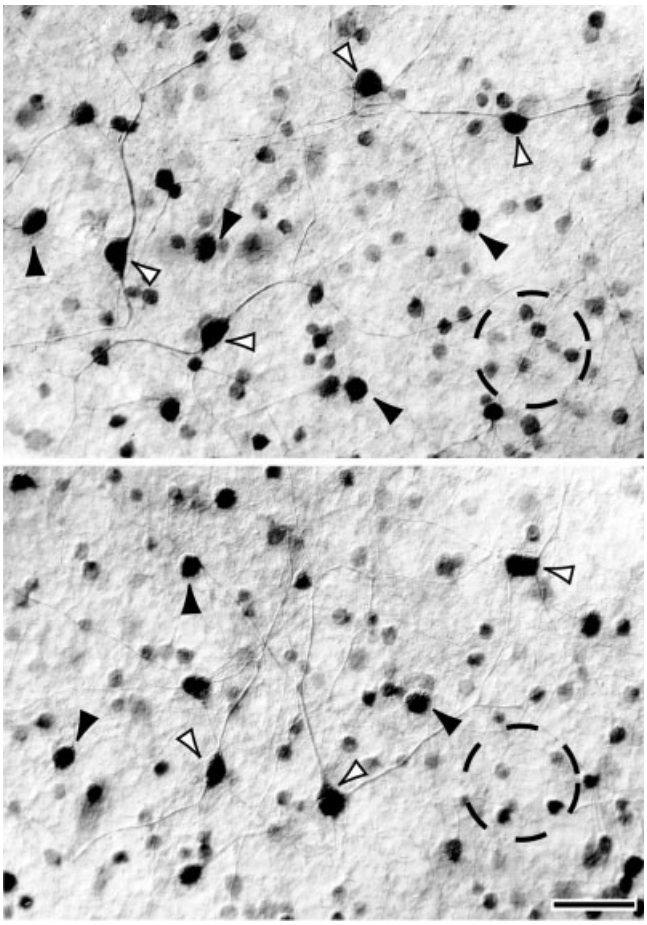

Fig. 1. Whole-mount preparation of macaque retina immunolabeled for αCamKII. A population of prominently labeled ganglion cells with large, sparsely branching dendritic trees (white arrowheads) is intermingled with a population of smaller labeled ganglion cells whose dendritic trees are less well articulated (black arrowheads). Lighter staining also outlines the somas of other ganglion and amacrine cells (outlined). Eccentricity: 12 mm temporal-superior of fovea. Scale bar = 20 μm.

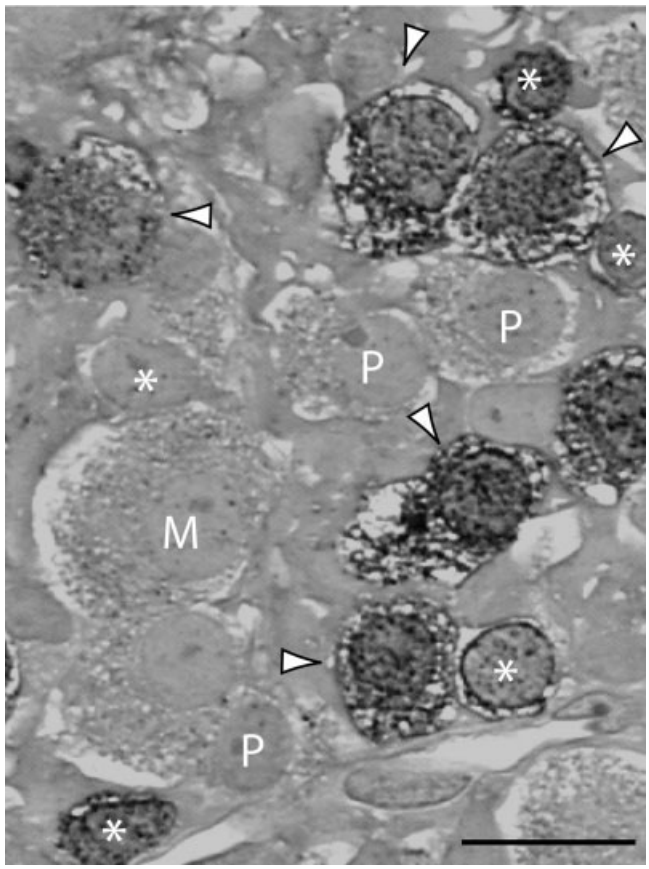

Fig. 2. Horizontal semithin section through the ganglion cell layer of a retina immunostained for αCamKII and counterstained with toluidene. Cells that are αCamKII+ are clearly distinguished from unlabeled cells by the presence of granular DAB product (arrowheads). Labeled cells are intermediate in size between larger, presumably magnocellular-projecting cells (M) and highly numerous and smaller, presumably parvocellular projecting cells (P). A group of amacrine cells is also labeled for αCamKII (asterisks). Eccentricity: 2 mm temporal-inferior to foveal center. Scale bar = 15 μm.

labeled cells, which rises prominently from the middle of the range, 240–250 μm^2, between clusters of the smallest (180–190 μm^2) and largest (400–600 μm^2) unlabeled cells. Thus, the somas of αCamKII+ ganglion cells are of intermediate size compared with the population of unlabeled cells.

αCamKII+ retinal ganglion cells form two morphological clusters

We asked next whether αCamKII-labeled ganglion cells represent multiple morphological types. First, we tested the distribution of somal areas in Figure 3 for multimodality by using the Kruskal "dip intensity" test (Giacomelli et al., 1971). This test measures the tendency of a distribution to deviate from a single peak to any number of peaks, depending on the context, and is independent of any underlying assumptions regarding the shape of the distribution or the location of its peaks. The value of the Kruskal statistic for the distribution in Figure 3 is 1.2 and does not reject the hypothesis of a unimodal distribution ($P > 0.5$). However, the morphology of the ganglion cells with clearly labeled dendritic trees does appear to indicate two broad groups. The first group demonstrates a broad, sparsely branching dendritic tree, with three or four primary dendrites emanating from a highly rounded cell body (Fig. 4). Ganglion cells of the second group have strictly two primary dendrites that emanate at about a 180° angle from a smaller, more elliptical cell body (Fig. 5). That these two morphologies represent at least two types of ganglion cell is supported by our observation that "rounded" and "elliptical" cells often appear side by side, notwithstanding the extreme diameters of their dendritic trees. Such large cells, were they of a unitary type, would be expected to sample the retina at much greater intervals to optimize their coverage (Sterling, 1998).

We sought to quantify the apparent difference in somal morphology by using a sample of αCamKII+ ganglion cells from the retinal periphery. We compared the size of each cell's soma with the aspect ratio, defined as the ratio of the major axis to the minor axis formed by the ellipse best fitting the soma. Higher aspect ratios indicate a more

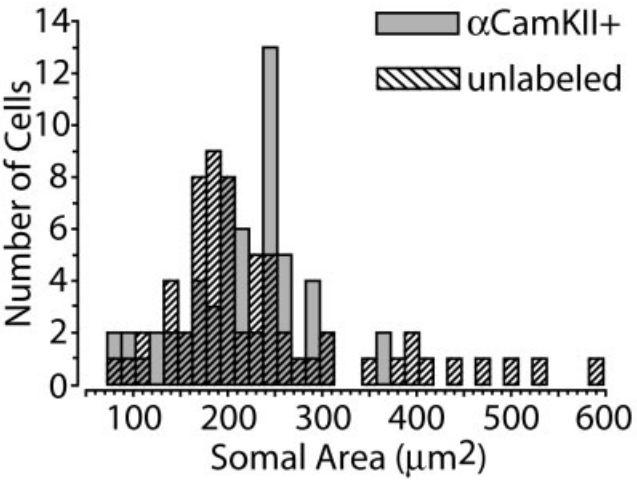

Fig. 3. Histogram of the somal area of 124 ganglion cells measured from horizontal semithin sections, as shown in Figure 2. The distribution of αCamKII+ cell bodies (mean ± SEM: 207.5 ± 8.0 μm^2, N = 61) is not significantly different from that of unlabeled cells (mean ± SEM: 229.1 ± 13.4 μm^2, N = 63; t = 1.4, $P = 0.17$).

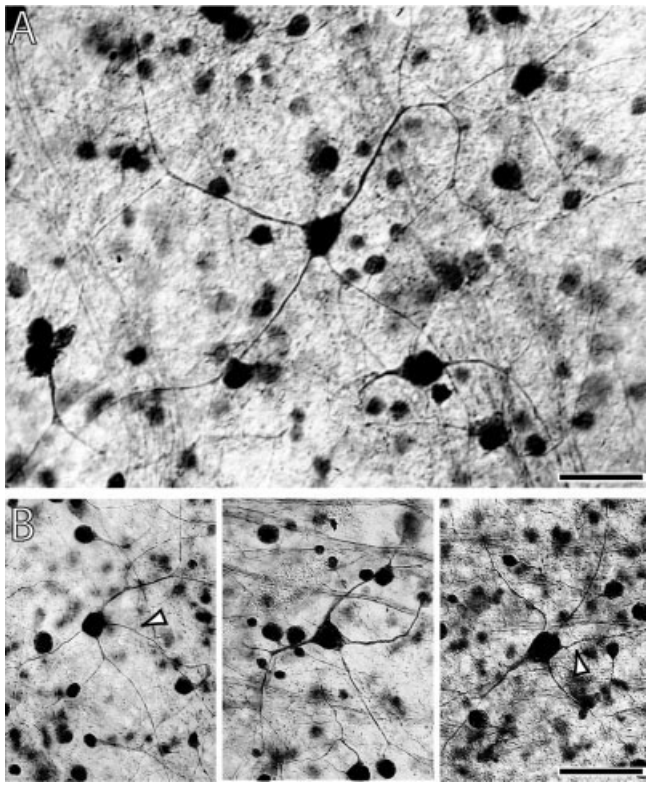

Fig. 4. αCamKII+ ganglion cells with rounded cell bodies and three or four primary dendrites. **A:** Example of a cell with a densely labeled dendritic tree exceeding 175 μm in diameter. Eccentricity: 6 mm temporal-superior to fovea. **B:** Three similar cells from the nasal-superior retina, 4–6 mm from the optic nerve head. An axon is clearly visible for two of the ganglion cells (arrowheads), and, in both A and B, bundles of stained axons are evident in the background. Scale bars = 25 μm in A; 50 μm in B.

elliptical soma, whereas an aspect ratio of 1 indicates a perfectly rounded soma. The scatterplot for this comparison indicates a strong negative correlation between the two properties, so that smaller cell bodies tend to be far more elliptical, whereas larger cell bodies tend to be rounder (Fig. 6A). The range for areas of cell bodies with an aspect ratio less than 1.5 is 225–390 μm^2 (mean ± SEM: 306.3 ± 10.0 μm^2), and the range for cell bodies with aspect ratio greater than 1.5 is 105–275 μm^2 (mean ± SEM: 204.0 ± 6.7 μm^2). The difference between the means for these two arbitrarily defined groups is statistically significant ($t = 8.8$, $P << 0.01$). To support these apparent differences, a histogram of aspect ratios from a larger sample clearly demonstrates two peaks, one near 1.2 (rounded somas) and one near 1.8 (elliptical somas; Fig. 6B). Correspondingly, the value of the Kruskal dip statistic for the distribution (2.4) indicates a significant tendency toward bimodality ($P < 0.05$).

Although we observed that rounded αCamKII+ ganglion cells always had three or more primary dendrites, the detailed morphology of their dendritic trees was quite variable (Fig. 4). Thus, pending additional studies with quantitative measurements, we cannot state with confidence how many distinct types of ganglion cell are included in this group. In contrast, the morphology of ganglion cells with a smaller, elliptical cell body is highly regular: strictly two primary dendrites separated by about 150–180° that stratify immediately along the border between the ganglion cell and inner plexiform layers (Fig. 7A,B). We then determined whether these two groups are distinguished by additional parameters. From our sample of αCamKII+ ganglion cells with a well-articulated dendritic tree and densely labeled and well-structured axon, we separated cells with three or more primary dendrites from those with strictly two. Cells with three or four primary dendrites ramify through a broad range of depths through the inner plexiform layer, nearly evenly divided between cells with dendrites in the inner 50% of the inner plexiform layer (ON sublamina) and cells with dendrites in the outer 50% (OFF sublamina; Fig. 7C, open circles). These cells categorically have rounded cell bodies (aspect ratio < 1.5). In contrast, ganglion cells whose morphology matches that of the reconstructions in Figure 7A ramify through a more narrow range of depth, with the majority of cells with dendrites in the ON sublamina (Fig. 7C, solid circles). The cells always have a somal aspect ratio >1.5.

Each αCamKII+ ganglion cell whose dendritic tree we were able to characterize in the fashion described above was monostratified in the sense that the primary dendrites emanated from the cell body to ramify in either the ON or the OFF sublamina, but not both. This contrasts with the small-bistratified ganglion cell described in earlier studies, with both primary dendrites that stratify in the ON sublamina and primary dendrites in the OFF (Dacey and Lee, 1994; Calkins et al., 1998). However, we cannot reject the possibility that dendrites less visible through weak staining coursed beyond the limits we measured for clearly labeled dendrites to breach both sublamina.

The two groups of αCamKII+ ganglion cell also differ with respect to axon diameter, measured at its broadest point near the cell body (Fig. 7D). Each ganglion cell with three or more primary dendrites and a somal aspect ratio <1.5 had a thick axon about 1.4 μm in diameter (mean ±

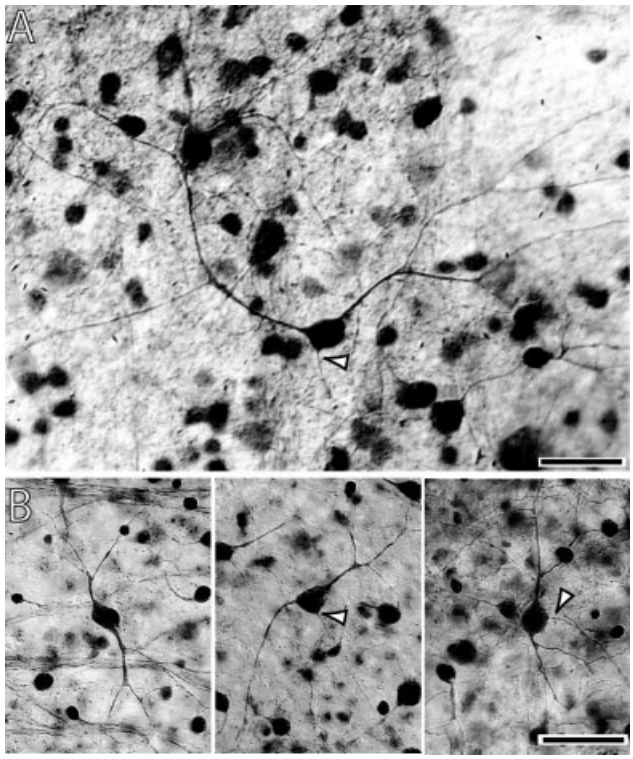

Fig. 5. A second group of αCamKII+ ganglion cells with elliptical cell bodies and two primary dendrites. **A:** Ganglion cell with sparsely branching dendritic tree about 200 μm in diameter. Eccentricity: 7 mm temporal-superior to fovea. **B:** Three additional cells from the nasal-superior retina, 4–6 mm from the optic nerve head. Axons, where apparent, are indicated by arrowheads. Scale bars = 25 μm in A; 50 μm in B.

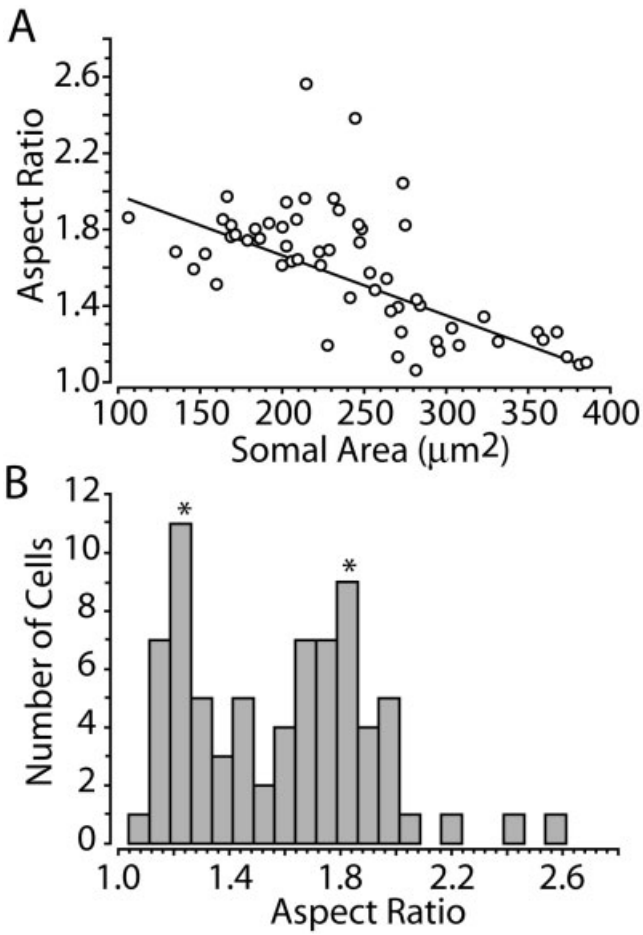

Fig. 6. The aspect ratio of αCamKII+ ganglion cell bodies forms a bimodal distribution. **A:** The aspect ratio decreases as a function of somal area for a sample of αCamKII+ ganglion cells from the peripheral retina. Line is best-fitting regression ($r = 0.42$, $P < 0.01$). **B:** Histogram of the aspect ratio of the cell bodies of these same ganglion cells demonstrates peaks near 1.2 and 1.8 (asterisks). Eccentricity: 7–9 mm nasal-superior of optic nerve head.

SEM: 1.41 ± 0.08 μm), whereas cells with two primary dendrites and an aspect ratio >1.5 had an axon about half as wide (mean ± SEM: 0.68 ± 0.06 μm). The difference between the means for the two groups is significant ($t = 7.5$, $P << 0.001$), even though our sample of clearly delimited axons was of limited size.

Finally, to establish the consistency of the morphology of elliptical αCamKII+ ganglion cells (e.g., Fig. 7A) throughout the retinal mosaic, we compared across eccentricities their somal aspect ratio with that of all other labeled cell bodies. Across a wide range of eccentricities, the difference in aspect ratio between the two groups remains remarkably consistent (Fig. 8A), with elliptical cells clustering near 1.8 (mean ± SEM: 1.80 ± 0.02) and all other cells near 1.2 (mean ± SEM: 1.23 ± 0.01); the difference is highly significant ($t = 34.4$, $P << .001$). Only a handful of labeled cells had an aspect ratio that exceeded that of elliptical ganglion cells at any given eccentricity. Most of these we confirmed to be amacrine cells because of the presence of a distended nucleus that filled an otherwise very small cell body (areas of 50–80 μm^2). We then used both aspect ratio (>1.5) and dendritic tree morphology (strictly two primary dendrites) to identify all elliptical ganglion cells along a strip of retina temporal to the parafovea (Fig. 8B), restricting our counts to those cells with visible dendrites confined to the ON sublamina. Although nearer the fovea the stacking of ganglion cell bodies into multiple levels prevented us from taking measurements, we could establish that elliptical cells, while highly regular in morphology, are nevertheless very rare and sample on average at a rate of only about 5 cells/mm^2 over most of the retina.

αCamKII+ axons in the optic nerve are intermediate in size and form a bimodal distribution

We questioned whether the expression of αCamKII in ganglion cell axons continues in the optic tract and, if so, whether the difference in axonal diameter suggested by our retinal studies (Fig. 7D) persists. Under the light microscope, in a given section of optic nerve, αCamKII label delineates some 10–15% of all axons (Fig. 9). However, this estimate is only from samples of nerve, generally from blocks of 150–175 μm in diameter. Sporadic penetration of the antibody, typical of myelinated tissue, prevented us from using complete cross-sections suitable for an absolute count. In these sections, the αCamKII+

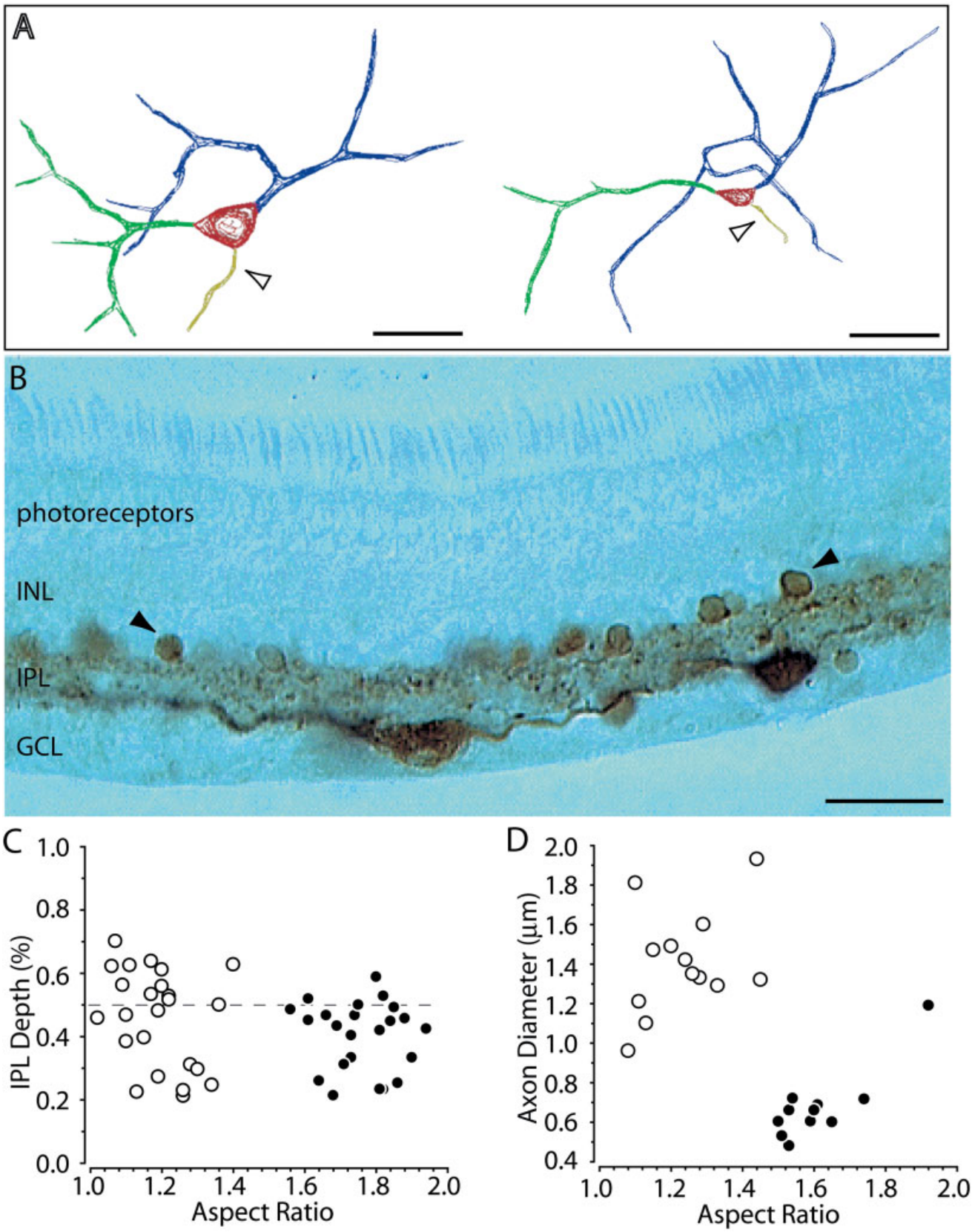
A
B
photoreceptors
INL
IPL
GCL
C
IPL Depth (%)
0.0
0.2
0.4
0.6
0.8
1.0
1.0
1.2
1.4
1.6
1.8
2.0
Aspect Ratio
D
Axon Diameter (µm)
0.4
0.6
0.8
1.0
1.2
1.4
1.6
1.8
2.0
1.0
1.2
1.4
1.6
1.8
2.0
Aspect Ratio

Figure 7

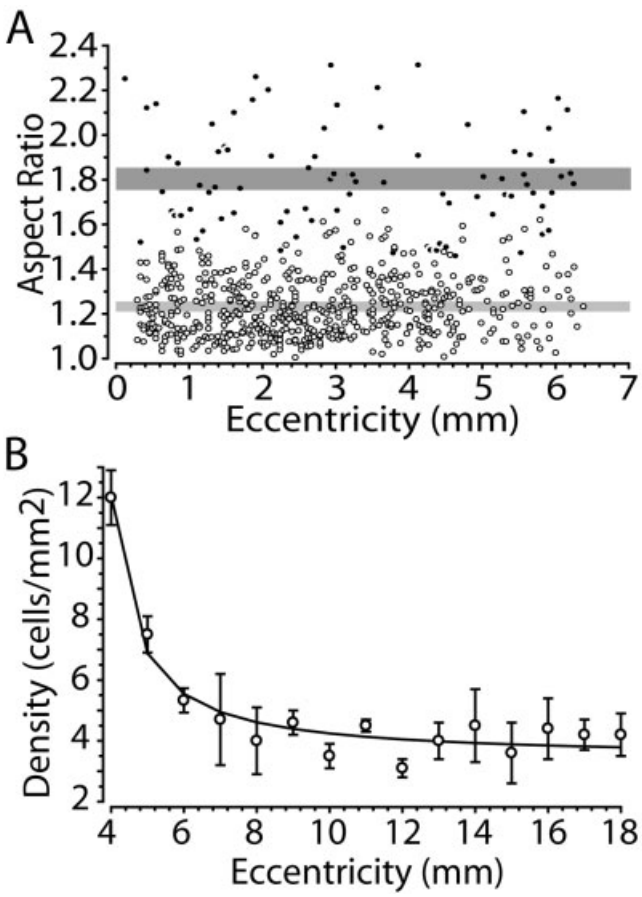

Fig. 8. Aspect ratio is consistent across eccentricity. **A:** Scatterplot of the aspect ratio of αCamKII+ cell bodies as a function of eccentricity from optic nerve head (nasal retina). Elliptical ganglion cells maintain a soma aspect ratio greater than 1.5 (solid circles), whereas all other labeled cells (both amacrine and ganglion) have a cell body with a much smaller aspect ratio (open circles). The 95% confidence intervals are indicated for both sets of cells (gray bars). **B:** Density of ganglion cells identified as elliptical (two primary dendrites, somal aspect ratio greater than 1.5) as a function of eccentricity from the fovea (temporal superior retina).

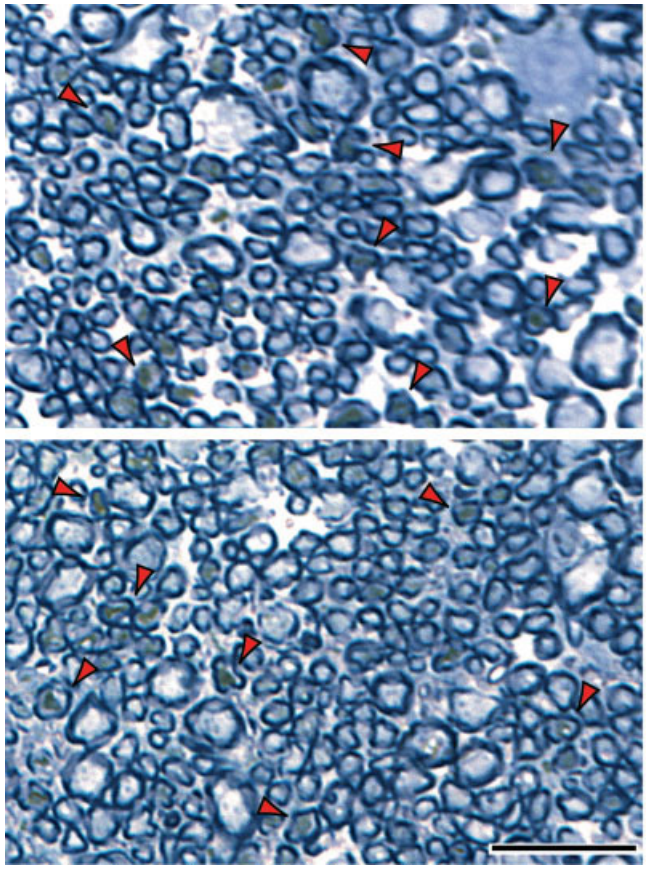

Fig. 9. High-magnification light micrographs of cross-sections through optic nerve immunostained for αCamKII and counterstained with toluidene (semithin sections prepared from Epon-embedded material; see Materials and Methods). Individual axons that are αCamKII+ are clearly distinguished from unlabeled axons by the presence of DAB product in the axonal interior (arrowheads). Labeled axons appear to be primarily of intermediate size. Scale bar = 10 μm.

Fig. 7. Morphology correlates with axon diameter. **A:** Reconstructions from multiple planes of focus through two examples of elliptical ganglion cells with axons indicated (arrowheads). The reconstructed dendritic trees, though only partial, are both greater than 100 μm in diameter. Main branches are indicated by separate colors for clarity. Eccentricity: 9 mm temporal to fovea. **B:** Vertical section (60 μm thick) cut through whole-mount preparation demonstrating narrow stratification of the two primary dendrites of an elliptical ganglion cell along the border of the ganglion cell layer (GCL) and inner plexiform layer (IPL). Section also indicates the population of labeled amacrine cells in the inner nuclear layer (INL; arrowheads). Eccentricity: 5 mm inferior to fovea. **C:** Depth of dendritic stratification between the GCL (0% depth) and INL (100% depth) compared with somal aspect ratio for αCamKII+ ganglion cells with three or four primary dendrites (open circles) and ganglion cells with strictly two primary dendrites (solid circles). Dotted line estimates ON and OFF subdivision of IPL. **D:** Axon diameter of ganglion cells with somal aspect ratio near 1 have large axons (open circles), whereas ganglion cells with higher somal aspect ratio have axons about 50% as broad (solid circles). Eccentricity (C,D): nasal-superior retina, 8–10 mm from the optic nerve head. Scale bars = 20 μm in left panel of A and in B; 30 μm in right panel of A.

axons appear intermediate in size between the largest diameter axons (presumably M) and the far more numerous smaller axons (presumably P; for review see Shapley and Perry, 1986). Under the electron microscope, most αCamKII+ axons appear about 0.4 μm in diameter, compared with diameters of 0.2 μm for the smallest of the unlabeled axons and 1.5 μm for the largest (Fig. 10). To compare the actual sizes of labeled and unlabeled axons, we measured the cross-sectional area of cytosol contained within the myelin sheath of about 2,400 axons, 15% of which were αCamKII+ (Fig. 11). The range for the area of unlabeled axons is quite large, 0.01–2.5 μm^2 (mean ± SEM: 0.37 ± 0.01 μm^2), whereas the range for the labeled axons is between these extreme values, 0.05–1.6 μm^2 (mean ± SEM: 0.44 ± 0.02 μm^2). That the peak value for the labeled axons is so much larger is indicative of the preponderance of small P cell axons in the unlabeled population.

The means for the labeled and unlabeled axons are statistically different, assuming that each is sampled from a uniform, normal distribution ($t = 3.03$, $P << 0.01$). However, in our electron micrographs, the size of αCamKII+ axons does not appear to be uniform (Fig. 10).

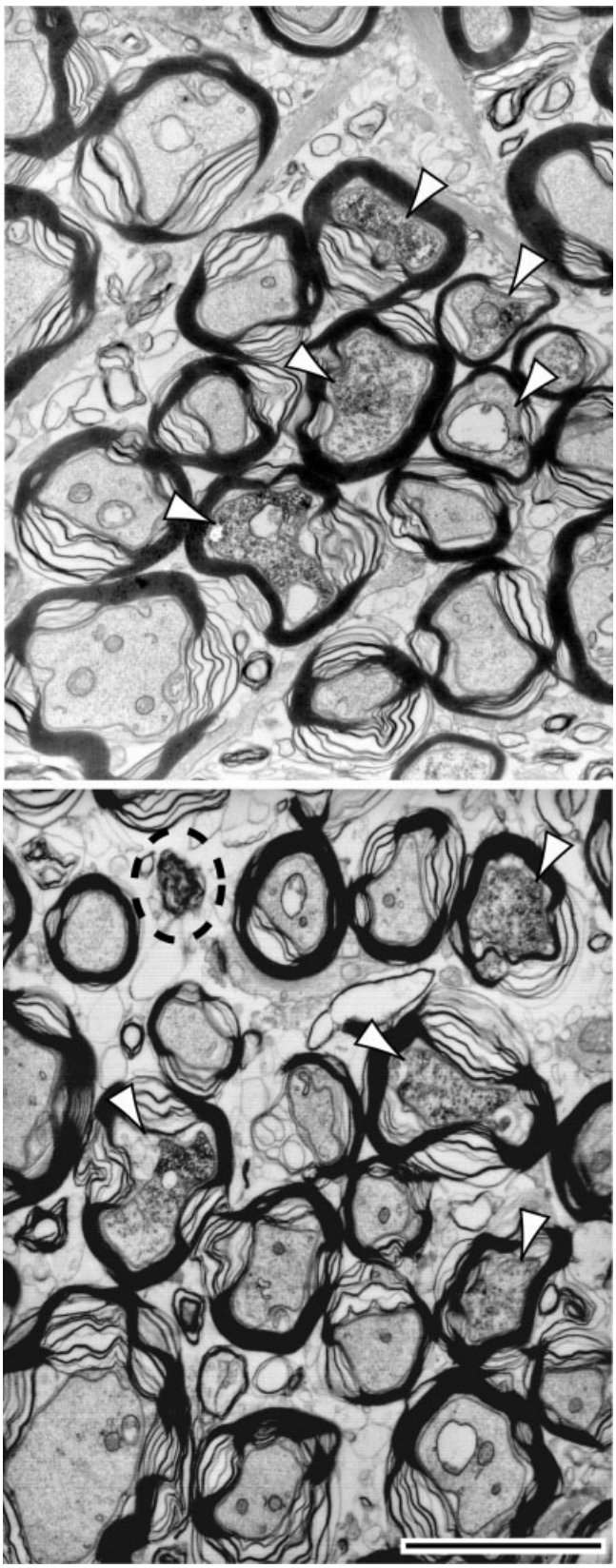

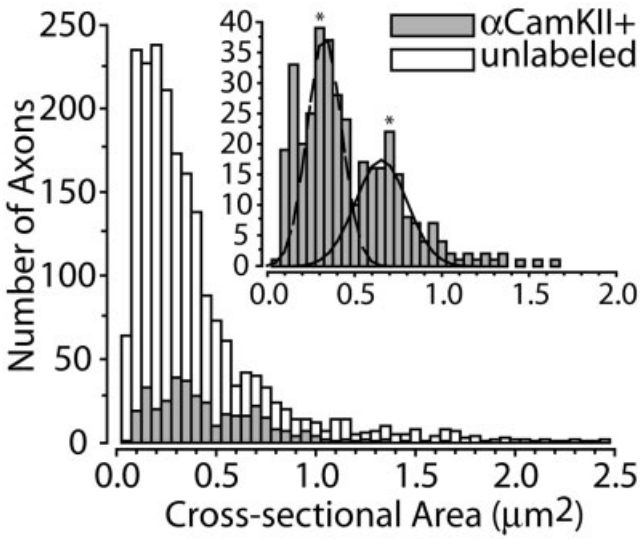

Fig. 11. The cross-sectional area of αCamKII+ axons forms a bimodal distribution. Histogram of cross-sectional area measured from 2,036 unlabeled and 366 labeled axons contained in our electron micrographs. The distribution of αCamKII+ axons (separated in **inset**) is bimodal, with peaks near 0.3 and 0.7 μm^2 (asterisks). This was verified statistically (see Results). The curves are independent Gaussians with means of 0.33 and 0.65 and standard deviations of 0.01 and 0.15, respectively.

The cross-sectional areas of labeled axons, when separated from the histogram of unlabeled axons (Fig. 11, inset), indeed form what appears to be a bimodal distribution of small (0.2–0.4 μm^2) and large (0.6–1.0 μm^2) axons. The value of the Kruskal dip statistic (1.64) rejects the null hypothesis that the axons are sampled from a unimodal distribution ($P < 0.01$). These results support the idea that the difference in axon size between the two populations of ganglion cell apparent in the retina persists in the optic nerve and is represented in the bimodal distribution formed by axonal diameter.

Synaptic input to K cells from αCamKII+ retinal terminals

The gross morphology of retinogeniculate input to the K layers has been described in detail for a variety of primate species (Tigges and Tigges, 1987; Conley and Fitzpatrick, 1989; Lachica and Casagrande, 1993; Johnson and Casagrande, 1995). The ultrastructure of synaptic terminals in the LGN is also well characterized. These form three major, though not exclusive, groups (RLP, F, and RSD) that are distinguished based on their size, the morphology of their synaptic vesicles and mitochondria, and their or-

Fig. 10. αCamKII+ axons in optic nerve are of intermediate diameter but variable in size. Electron micrographs of immunostained optic nerve (same tissue as in Fig. 9). Labeled axons were identified by the presence of granular DAB reaction product (arrowheads) and appear to be intermediate in size relative to unlabeled axons, but also variable (compare labeled axons in bottom panel). Fibers without clear myelination (dashed circle) were excluded from further analysis, because these could arise from immunolabeled glial processes. Scale bar = 2 μm.

igin (for review see Guillery, 1971; Wilson, 1993). Most pertinent to this study are RLPs, which arise from the axonal terminations of retinal ganglion cells and are identified by their generally large size relative to other synaptic terminals in the LGN and by their rounded vesicles and relatively pale mitochondria (Wilson and Hendrickson, 1981; Feig and Harting, 1994). The F terminals, in contrast, arise primarily from inhibitory interneurons in the LGN and have flattened, pleomorphic vesicles; some (the F2 subtype) form synaptic triads involving reciprocal connections with RLPs and LGN relay neurons. F terminals also demonstrate darker mitochondria and paler cytoplasm. The RSD terminals are almost uniformly the smallest of the presynaptic terminals in the LGN, generally characterized by a dense packing of synaptic vesicles. These are mostly cortical in origin, although some RSD terminals in the koniocellular layers of the primate LGN arise from sources in the brainstem, especially the superior colliculus (Harting et al., 1991; Feig et al., 1992; for review see Casagrande, 1994; Hendry and Reid, 2000).

We used this morphological scheme to investigate whether the expression of αCamKII in ganglion cell axons of the optic nerve continues in the LGN, in particular, in proximity to αCamKII+ K cells (Fig. 12). This is a challenging question, given the diversity in the sizes and morphology of the three primary groups of axon terminal and the chance that subgroups of each of type could express αCamKII. Complete quantification requires a rigorous, stereological analysis combined with retrograde filling of terminals that we did not attempt for this study. Nevertheless, a broad survey of the neuropil near an αCamKII+ neuron in K4 demonstrates that the stained dendrites of these cells receive many synaptic contacts from all three classes of major LGN terminal (Fig. 12). Some generalities are apparent. By far the most frequent contacts are from RSD and F terminals, often in combination to the same dendrite. The morphology and size of RSD terminals in particular are remarkably consistent. These terminals form elongated contacts marked by a large presynaptic active zone surrounded by a dense packing of vesicles that tends to fill the entire terminal. Indeed, only rarely did an RSD terminal forming a synaptic contact with an αCamKII+ dendrite contain mitochondria. In contrast, F terminals in our material—as in previous studies (Wilson, 1993)—have less densely packed vesicles and presynaptic densities often flanked by one or more dark mitochondria. About half of the RSD terminals in our survey appear significantly more electron dense than the F terminals, suggesting the presence of DAB reaction product and the expression of αCamKII. Finally, whereas F terminals appear only slightly larger than RSD terminals, RLP terminals in contrast are consistently larger than both by a factor of two to three. Even so, in our material, terminals that are presynaptic to αCamKII+ dendrites in the K layers that we would classify as RLP can appear smaller in single cross-sections than either F or RSD terminals (Fig. 13A). For these cases, we were able to distinguish RLPs based on their configuration in synaptic triads with F2 terminals or by their generally paler mitochondria (Fig. 13A).

These morphological criteria are hardly infallible and must be used in combination to guide the discrimination of RLPs from other terminals. We did so to make a more detailed examination of the RLPs contacting αCamKII+ neurons. This survey revealed an interesting trend. Typically, in a single ultrathin section, an αCamKII+ dendrite receives multiple synapses from a combination of RLP, F, and RSD terminals (Fig. 13A). Among these are RLPs that are *themselves* αCamKII+, most often forming a long, filamentous active zone with the labeled dendrite (Fig. 13B–D). In some cases, these RLPs contact the cell body of an αCamKII+ neuron directly (Fig. 14), again forming a lengthy, filamentous contact. The size of these αCamKII+ terminals greatly exceeds that of typical RSD terminals, and, because interneurons in the LGN do not express αCamKII, we would not expect F terminals to contain immunolabel. By examining each morphologically unambiguous RLP in our electron micrographs, we found that the fraction of those containing αCamKII increases significantly in moving from the dorsal layers (K6–K4) to the ventral layers (K1–K2). We identified in our sample of RLPs in K6 and K5 less than 10% expressing αCamKII, whereas in K1 and K2 the fraction increases to just over 45% (Fig. 15). These observations can be appreciated by comparing the large number of unlabeled RLPs in Figure 12 (K4) with the labeled RLPs in Figures 13 and 14 (K1 and K2).

DISCUSSION

An αCamKII+ projection from the retina to the koniocellular LGN

Perhaps our most intriguing finding is that the same αCamKII signature that delineates the population of koniocellular neurons in the LGN also characterizes multiple ganglion cell pathways, one or more of which provides retinal input to at least some K cells. This neurochemical signature begins in the retina with the dendritic arbors of at least two types of ganglion cell (Figs. 1–8), continues in the optic nerve (Figs. 9–11), and terminates in the LGN at least partially with RLP contacts to αCamKII+ dendrites in the koniocellular LGN (Figs. 12–14). This projection is defined broadly in the retina by ganglion cells whose size, in terms of somal area, is intermediate between that of M (parasol) and P (midget) cells (Fig. 3) and in the optic nerve by axons also of intermediate size (Fig. 11).

We apply the term "signature" loosely, for certainly our data indicate that this αCamKII+ projection is likely to represent multiple pathways to the brain. In the retina, a subset of small, αCamKII+ ganglion cells lacks robust labeling in either their dendritic trees or, more importantly, in their axons (Fig. 1). Thus, we are tacitly excluding them from this projection. Even so we must acknowledge that there is no a priori reason why ganglion cells with weak or even absent labeling in the retina would also have correspondingly weak or absent label in their axons. Expression levels of αCamKII could easily depend on transcription events that vary from dendritic to axonal localization. Conversely, we know that some ganglion cells that appear to lack αCamKII expression altogether do project to the koniocellular LGN (see below).

Those αCamKII+ ganglion cells with robust label are distributed into two main groups, both with sparsely branching, broad dendritic trees. Some cells have three or four primary dendrites and a thick axon emanating from a round cell body; other cells have strictly two primary dendrites and a thinner axon emanating from an elliptical cell body (Figs. 4, 5). These two groups are statistically separable in terms of both somal aspect ratio and axonal

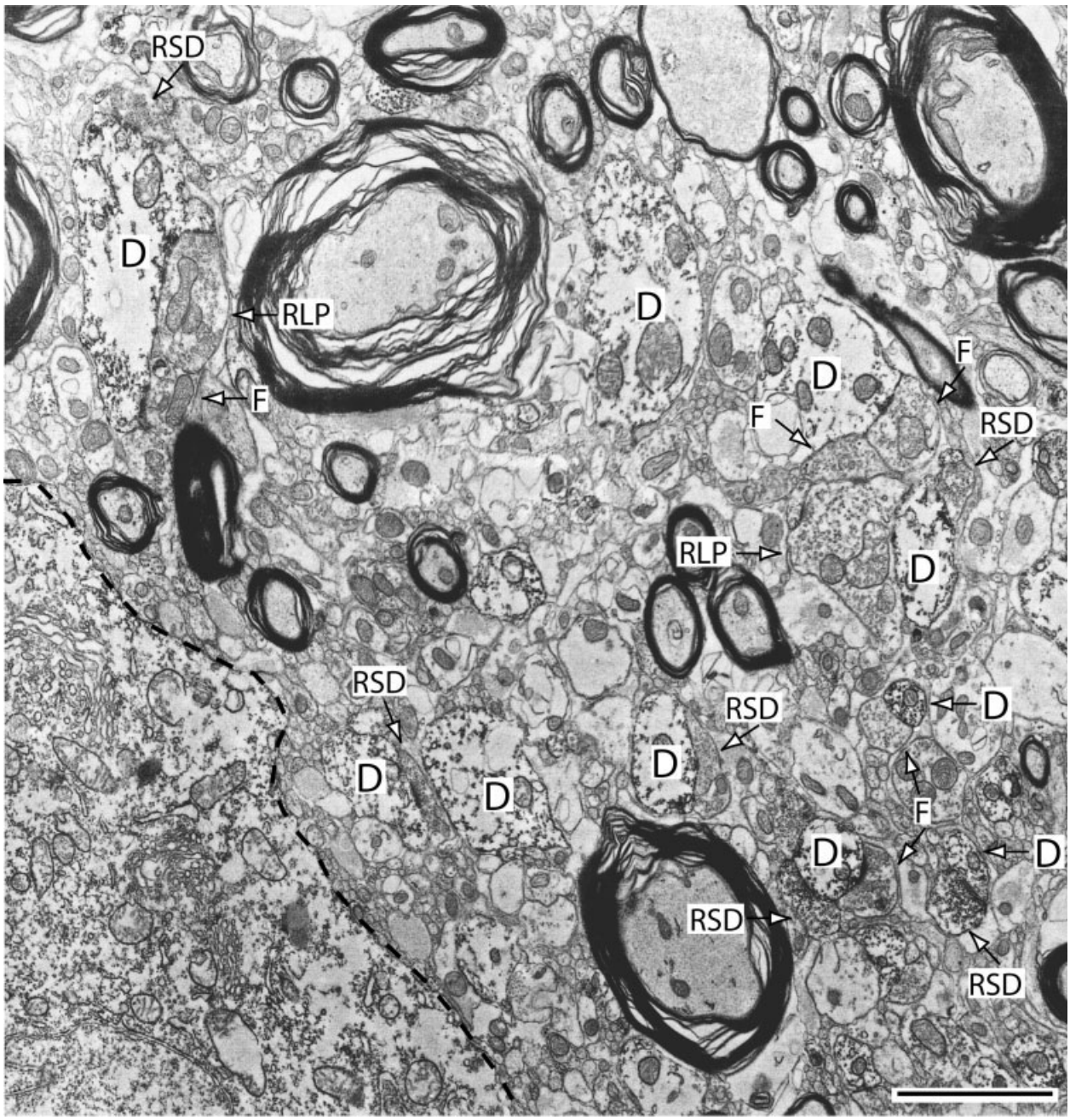

Fig. 12. Dendrites of αCamKII+ neurons in LGN are postsynaptic to all types of major axonal terminals. Low-magnification electron micrograph of αCamKII+ neuron (dashed outline) and dendrites in K4 identified by the presence of granular DAB product. Multiple αCamKII+ dendrites (D) near this neuron receive synapses from retinal afferents (RLP) and from RSD and F terminals arising from various sources (see Wilson, 1993). Scale bar = 2 μm.

diameter (Figs. 6, 7). Our finding that αCamKII+ axons in the optic nerve are bimodally distributed supports the breakdown of labeled ganglion cells into two groups, although axonal diameter is bound to vary even within a sample of a single cell type. Most optic nerve axons with αCamKII are intermediate in size between the largest and smallest unlabeled axons. The cross-sectional area for unlabeled axons spanned a range of 0.01–2.5 μm^2, whereas the area for αCamKII+ spanned a range about half that size (0.05–1.6 μm^2). This would imply that the conduction velocities of αCamKII+ ganglion cells also tend to be intermediate between those of the faster M and slower P cells (see Shapley and Perry, 1986).

The ganglion cells that we have called "rounded" have multiple morphologies, which we did not attempt to separate in this study, so these cells probably include several types. Many of these cells have dendritic arbors at least 150–200 μm in diameter in the retinal periphery (Figs. 1,

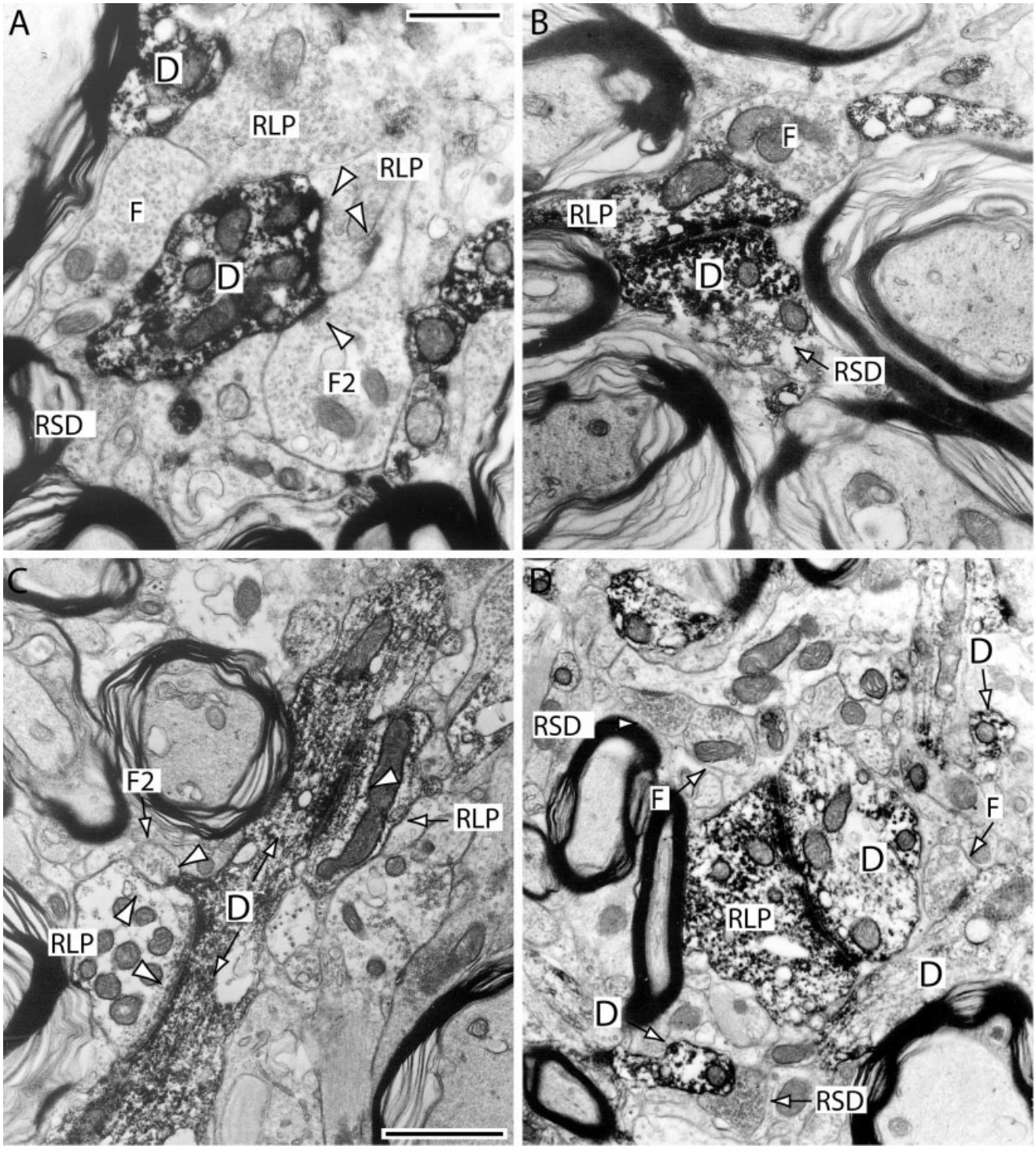

Fig. 13. Retinal afferents to αCamKII+ neurons are often themselves αCamKII+. **A:** Electron micrograph of an αCamKII+ dendrite (D) postsynaptic to what is likely a small RLP and an F2 terminal, both identified by the formation of a synaptic triad (arrowheads). An RSD terminal also contacts the dendrite (lower left). A larger RLP is presynaptic to a second αCamKII+ dendrite (upper left). **B:** An αCamKII+ RLP forms a filamentous contact with a labeled dendrite. **C:** Two labeled RLPs form long filamentous contacts (arrowheads) with a αCamKII+ dendrite. The RLP at lower left also contacts an F2 terminal, which forms a triad by contacting the dendrite. **D:** Another example of a large αCamKII+ RLP forming a filamentous contact with a labeled dendrite (D). An RSD terminal contacts a second αCamKII+ dendrite (lower left), and a small F terminal is presynaptic to a longer labeled dendrite (lower right). Neighboring RSD and F terminals (unlabeled, upper right) demonstrate the morphological differences between the two. All micrographs from layers K1 and K2. Scale bars = 1 μm in A (applies to A,B); 2 μm in C (applies to C,D).

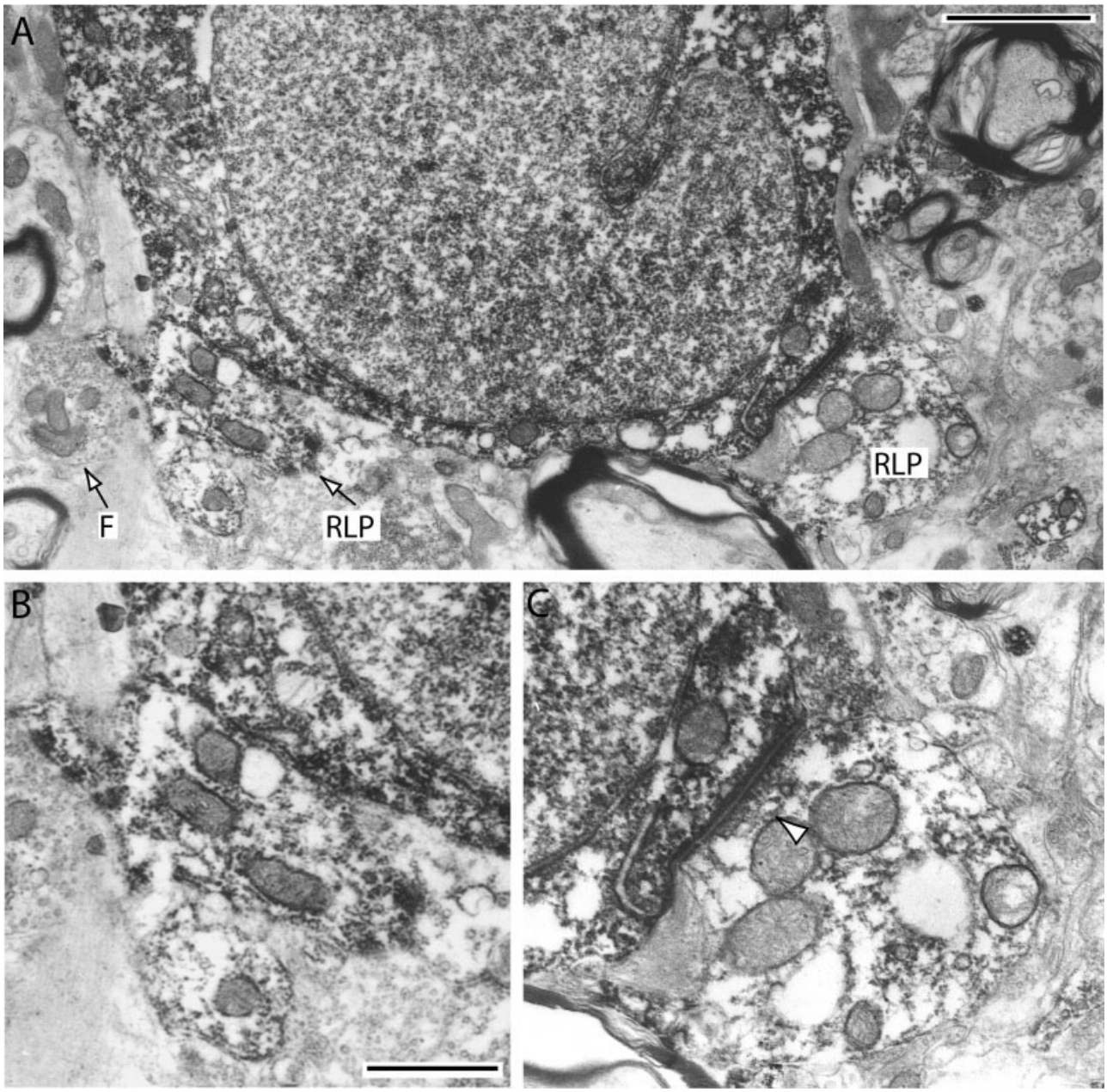

Fig. 14. αCamKII+ RLPs contact K cells directly. **A:** Cell body of αCamKII+ neuron receiving contact from two αCamKII+ RLP terminals. **B,C:** Higher magnification images of the RLPs in A. The RLP in C clearly provides a filamentous synapse to the cell body (arrowhead). Micrograph from K1. Scale bars = 2 μm in A; 1 μm in B (applies to B,C).

4), which, together with their general branching pattern, would place them in the "large sparse" category identified recently by retrograde labeling from the macaque LGN (Dacey et al., 2003). A subset of these cells also resembles the "ϵ" ganglion cell identified by intracellular injections of the macaque retina (Rodieck and Watanabe, 1993). In contrast, the ganglion cells we have called "elliptical" are far more regular in morphology, with their primary dendrites invariably forming about a 150–180° angle (Figs. 5, 7). We were able to use this branching pattern together with somal aspect ratio to distinguish these cells across retinal eccentricities and estimate their sampling properties (Fig. 8). These elliptical cells are similar to other sparsely branching ganglion cells, in particular, the wide-field, "large sparse" cell identified in the same retrograde labeling study (see Fig. 4A of Dacey et al., 2003), the "sparse diffuse" cell of the human retina identified by intracellular injection (see Fig. 7B of Peterson and Dacey, 2000), and the large "G3" and "G21" cells identified by Golgi impregnation of the human retina (Kolb et al.,

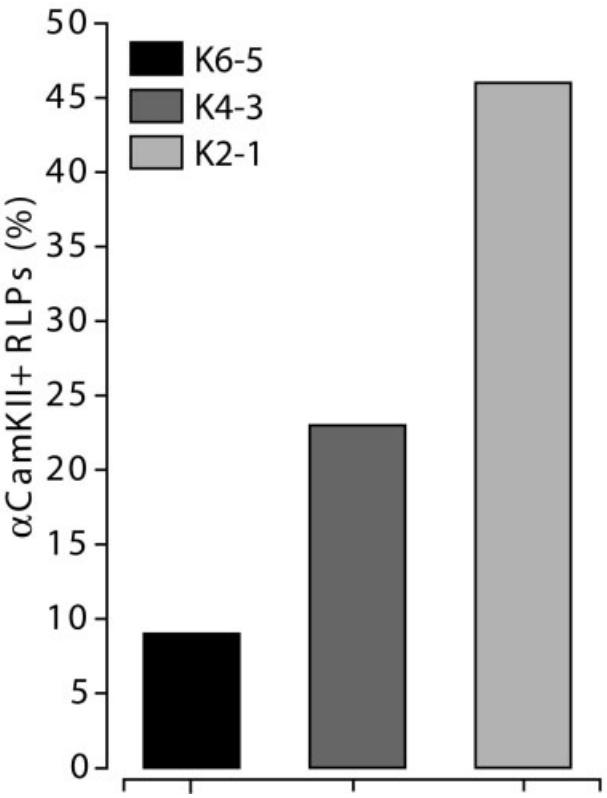

Fig. 15. Fraction of αCamKII+ RLPs identified in K1–K6 through our collection of high magnification electron micrographs (e.g., Figs. 13, 14). Incidence increases from the dorsal to ventral koniocellular layers. We identified a group of 120 RLPs based on clear morphological features as described in the text.

1992). These same cells also bear a striking resemblance to the "γ" ganglion cell described by others (Rodieck and Watanabe, 1993; Cowey et al., 1994).

Sampling properties of αCamKII+ pathways

Of key importance in linking a visual pathway to a psychophysical channel is establishing the rate at which the underlying neurons sample the spatial plane of the retina. For example, to account for the spatial resolution of the blue/yellow color channel, the small-bistratified ganglion cell, whose receptive field is tuned to blue/yellow spectral differences (Dacey and Lee, 1994), need only make up some 3–5% of all ganglion cells (Calkins, 2001). Our samples of optic nerve prepared for electron microscopy contained 15% αCamKII+ axons, about twice the fraction of the M-projecting, parasol ganglion cell (Grünert et al., 1993). In the whole-mount preparation from which we measured somal aspect ratio (Fig. 8), the elliptical ganglion cell represented about 15% of all αCamKII+ ganglion cells, which would correspond to roughly 2% of the axons in the optic nerve. In the retina, the axon hillock of this ganglion cell was about 50% as thick as the hillock of other labeled ganglion cells (Fig. 7D). Based on these numbers, one would expect the smallest αCamKII+ axons in the optic nerve to be far less frequent than the largest. However, in our sample of 366 αCamKII+ axons, those less than 0.5 μm^2 in cross-sectional area are nearly twice as frequent as those greater than 0.5 μm^2 (Fig. 11). One likely reason for this discrepancy is that, for the sample of ganglion cells from which we measured axon diameter (Fig. 7D), we biased our selection of nonelliptical cells in favor of the largest cells with the most clearly articulated proximal dendrites. Another contributing factor could be that some of the smallest of the labeled ganglion cells whose dendritic trees we could not discern do indeed have an αCamKII+ axon in the optic nerve. Admittedly, this possibility renders tenuous our link between the ganglion cells whose dendritic morphology we carefully described and the αCamKII+ RLP terminals in the LGN.

The apparently low fraction of elliptical ganglion cells based on αCamKII staining is not surprising, given that the peak density of these cells near the fovea cannot be more than 20–25 cells/mm^2 (Fig. 8). Under the assumption that the coverage factor (the product of dendritic field area and density) for these cells is unity, this sampling density would correspond to a dendritic tree diameter of about 200 μm in the central retina. With a coverage factor closer to three or four, as is generally the case for larger ganglion cells (Wässle and Boycott, 1991; Dacey and Brace, 1992; Dacey and Petersen, 1992; Dacey, 1993), this sampling density would correspond to a diameter of 350–500 μm. These cells could therefore span a distance three to seven times greater than the diameter of the parasol ganglion cell (Rodieck and Watanabe, 1993). The estimated size of the elliptical ganglion cell based on this range of coverage factors is therefore consistent with measurements placing the percentage of parasol cells at 5–8% (Grünert et al., 1993).

Stereological estimates of the number of K cells in the macaque LGN place their fraction in the neighborhood of 10% (Hendry and Reid, 2000). Several anatomical and physiological observations indicate that at least a subset of K cells in the intermediate zone of the LGN (K3–K4) receives retinal input from the small-bistratified ganglion cell (Martin et al., 1997; White et al., 2001; Solomon et al., 2001; Chatterjee and Callaway, 2002; Dacey et al., 2003). We did not identify the small-bistratified cell among those retinal ganglion cells overtly expressing αCamKII. Under the assumption that each small-bistratified cell (3–5%) corresponds to a single K cell in K3–K4 and that each elliptical cell (2%) definitively projects to another subset of K cells, our results would seem to imply that no more than 30% of the αCamKII+ axons from nonelliptical cells in the optic nerve can provide retinal input to the remaining 3–5% of K cells. It is therefore likely that many αCamKII+ ganglion cells project either to the M and P layers of the LGN or to one or more other subcortical structures deriving direct retinal input, some of which also contain αCamKII+ axon terminals (Benson et al., 1991). However, these numbers must be interpreted with some caution. Both the fraction of K cells and the fraction of small-bistratified cells are estimates that are subject to the same high degree of interanimal and interspecies variability that compels a great deal of caution in forming conclusions about the absolute number of neurons and optic nerve fibers projecting to the LGN (Spear et al., 1996).

Although the elliptical ganglion cell we describe here closely resembles the "large sparse" cell described from retrograde labeling of ganglion cells from the LGN in macaque (Fig. 4A of Dacey et al., 2003), in the above

analysis we must also acknowledge the strong possibility that either these cells or another subset of αCamKII+ ganglion cells project to other brain regions. In previous retrograde labeling studies, a morphologically diverse set of cells collectively known as "γ" was found to project to the pulvinar, pretectum, and superior colliculus (Cowey et al., 1994; see also Rodieck and Brening, 1983). It is also possible that axonal collaterals from LGN-projecting γ cells also terminate in these structures. However, another study of ganglion cell projections coupled with very detailed intracellular filling failed to find evidence of γ cells terminating in either the pretectum or the superior colliculus (Rodieck and Watanabe, 1993). These comparisons are especially meaningful given the morphological similarity among the canonical γ cell, the "large sparse" cells of Dacey et al. (2003), and the elliptical ganglion cells described here. A key experiment would be to test ganglion cells retrogradely labeled from the LGN (or from specific koniocellular layers) for αCamKII immunoreactivity.

Circuitry of αCamKII+ neurons in the koniocellular LGN

Relay neurons of the K layers provide a robust projection to the cytochrome oxidase-rich blobs of layer III of the primary visual cortex (V1; for review see Casagrande, 1994, 1999; Hendry and Reid, 2000). Because the blobs have been implicated in color discrimination (Livingstone and Hubel, 1984; Ts'o and Gilbert, 1988), there has been great interest in linking K cells with the blue/yellow and red/green color pathways to the cortex (Calkins and Sterling, 1999; Shostak et al., 2002). Certain other primates with K cells are likely to lack a blue/yellow pathway altogether because of the absence of short-wavelength-sensitive cones (Jacobs et al., 1993, 1996), so there is no a priori reason to link all K pathways with a functional role in color discrimination (Shostak et al., 2002). Indeed, there are remarkable similarities in K pathways to the cortex between diurnal and nocturnal primates (Xu et al., 2001).

It is tempting to refer to all αCamKII+ neurons in the LGN as "K" cells, implying a unitary class of relay neuron deriving retinal input from a single type of ganglion cell. However, several lines of evidence argue against this simplification. In the owl monkey (*Aotus*), neurons from different K layers form morphologically distinct projection patterns in V1 and demonstrate different spatiotemporal contrast sensitivity (Ding and Casagrande, 1997; 1998; Xu et al., 2001). In this nocturnal species, which lacks expression of the S-cone gene (Jacobs et al., 1993, 1996), layer K4 is seemingly absent (Hendry and Reid, 2000). Other differences exist among primate species in terms of the specific innervation of different K layers from the superior colliculus (Harting et al., 1991). These comparisons in total imply a certain degree of functional specificity for each K layer that depends on a variety of species-dependent factors.

Our results here indicate that retinal afferents near αCamKII+ neurons in macaque LGN form dense clusters in proximity to the cell body of these neurons (Figs. 12–14). These axon terminals form small, en passant swellings that resemble the basic structure of those observed in the K layers of the prosimian bushbaby (*Galago*; Lachica and Casagrande, 1993; Feig and Harting, 1994). We also observed a great deal of heterogenity in both the absolute size and the morphology of these terminals in moving from the dorsal to ventral K layers (compare Fig. 12 with Figs. 13, 14), which is consistent with results from the bushbaby. Some of these retinal terminals are themselves αCamKII+ (Figs. 13, 14), in a trend that increases in frequency moving from the dorsal K layers to the ventral (Fig. 15). These terminals also form direct presynaptic contact with the cell body of αCamKII+ neurons, in contrast to the circuitry in *Galago,* in which RLPs most often innervate distal regions of K cells (Feig and Harting, 1994). The lesser frequency of αCamKII+ RLPs in K3 and K4 is consistent with our observation that the small-bistratified ganglion cell does not express levels of αCamKII sufficient for identification by immunocytochemistry (see above).

Our claim that certain αCamKII+ terminals in the LGN correspond to RLPs is based primarily on their large size compared with RSDs and F terminals. However, it is possible—though we think not likely—that some of the terminals we scored as RLPs could represent large RSDs from noncortical sources, such as the superior colliculus, known to provide input the K layers (Feig and Harting, 1994). Sometimes, albeit rarely, a large, labeled RLP-like terminal demonstrated mitochondria that were darker than expected, a feature generally associated with RSD terminals (Fig. 13C). Our broad survey indicates that αCamKII+ neurons receive numerous contacts from both RSD and F terminals (e.g., Figs. 12, 13), both of which are far more numerous than contacts from RLPs. This is similar to the distribution of terminals in the primary layers of both primates and other mammals (see discussion in van Horn et al., 2000). We also observed a number of small RSD-like terminals that were also αCamKII+ (see Benson et al., 1991). A more thorough electron microscopy study is necessary to determine how this distribution changes across the K layers and whether the pattern of synaptic connections between these terminals and αCamKII+ cells demonstrates other, more telling neurochemical features, such as those that distinguish connections in the superior colliculus (Mize, 1999).

ACKNOWLEDGMENTS

We sincerely thank Leslie Meszler and Karen Bentley for their expertise, extraordinary patience, and assistance with electron microscopy and Prof. Vivienne Casagrande of Vanderbilt University for her extremely helpful and insightful comments on an early version of the article.

LITERATURE CITED

Benson DL, Isackson PJ, Hendry SH, Jones EG. 1991. Differential gene expression for glutamic acid decarboxylase and type II calcium-calmodulin-dependent protein kinase in basal ganglia, thalamus, and hypothalamus of the monkey. J Neurosci 11:1540–1564.

Calkins DJ. 2001. Seeing with S cones. Prog Ret Eye Res 20:255–287.

Calkins DJ, Sterling P. 1999. Evidence that circuits for spatial and opponent color vision segregate at the first retinal synapse. Neuron 24:313–321.

Calkins DJ, Tsukamoto Y, Sterling P. 1998. Microcircuitry and mosaic of a blue-yellow ganglion cell in the primate retina. J Neurosci 18:3373–3385.

Casagrande VA. 1994. A third parallel visual pathways to primate area V1. Trends Neurosci 17:305–310.

Casagrande VA. 1999. The mystery of the visual system K pathway. J Physiol 517:630.

Chatterjee S, Callaway EM. 2002. S cone contributions to the magnocellular visual pathway in macaque monkey. Neuron 35:1135–1146.

Conley M, Fitzpatrick D. 1989. Morphology of retinogeniculate axons in the macaque. Vis Neurosci 2:287–296.

Cowey A, Stoerig P, Bannister M. 1994. Retinal ganglion cells labeled from the pulvinar nucleus in macaque monkeys. Neuroscience 61:691–705.

Dacey DM. 1993. Morphology of a small field bistratified ganglion cell type in the macaque and human retina. Vis Neurosci 10:1081–1098.

Dacey DM, Brace S. 1992. A coupled network for parasol but not midget ganglion cells in the primate retina. Vis Neurosci 9:279–290.

Dacey DM, Lee BB. 1994. The "blue-on" opponent pathway in primate retina originates from a distinct bistratified ganglion cell type. Nature 367:731–735.

Dacey DM, Petersen MR. 1992. Dendritic field size and morphology of midget and parasol ganglion cells of the human retina. Proc Natl Acad Sci U S A 89:9666–9670.

Dacey DM, Peterson BB, Robinson FR, Gamlin PD. 2003. Fireworks in the primate retina: in vitro photodynamics reveals diverse lgn-projecting ganglion cell types. Neuron 37:15–27.

DeYoe EA, Van Essen DC. 1988. Concurrent processing streams in monkey visual cortex. Trends Neurosci 11:219–226.

Ding Y, Casagrande VA. 1997. The distribution and morphology of LGN K pathway axons within the layers and CO blobs of owl monkey V1. Vis Neurosci 14:691–704.

Ding Y, Casagrande VA. 1998. Synaptic and neurochemical characterization of parallel pathways to the cytochrome oxidase blobs of primate visual cortex. J Comp Neurol 391:429–443.

Felleman DJ, Van Essen DC. 1991. Distributed hierarchical processing in the cerebral cortex. Cereb Cortex 1:1–47.

Feig S, Harting JK. 1994. Ultrastructural studies of the primate lateral geniculate nucleus: morphology and spatial relationships of axon terminals arising from the retina, visual cortex (area 17), superior colliculus, parabigeminal nucleus, and pretectum of *Galago crassicaudatus*. J Comp Neurol 343:17–34.

Feig S, Van Lieshout DP, Harting JK. 1992. Ultrastructural studies of retinal, visual cortical (area 17), and parabigeminal terminals within the superior colliculus of *Galago crassicaudatus*. J Comp Neurol 319: 85–99.

Giacomelli F, Wiener J, Kruskal JB, Pomeranz JV, Loud AV. 1971. Subpopulations of blood lymphocytes demonstrated by quantitative cytochemistry. J Histochem Cytochem 19:426–433.

Goodchild AK, Martin PR. 1997. The distribution of calcium-binding proteins in the lateral geniculate nucleus and visual cortex of a New World monkey, the marmoset, *Callithrix jacchus*. Vis Neurosci 15:625–642.

Grünert U, Greferath U, Boycott BB, Wässle H. 1993. Parasol (Pα) ganglion-cells of the primate fovea: immunocytochemical staining with antibodies against $GABA_A$-receptors. Vis Res 33:1–14.

Guillery RW. 1971. Patterns of synaptic interconnections in the dorsal lateral geniculate nucleus of cat and monkey: a brief review. Vis Res Suppl 3:211–227.

Harting JK, Huerta MF, Hashikawa T, van Lieshout DP. 1991. Projection of the mammalian superior colliculus upon the dorsal lateral geniculate nucleus: organization of tectogeniculate pathways in nineteen species. J Comp Neurol 304:275–306.

Hendry SHC, Calkins DJ. 1998. Neuronal chemistry and functional organization in primate visual system. Trends Neurosci 21:344–349.

Hendry SHC, Reid RC. 2000. The koniocellular pathway in primate vision. Annu Rev Neurosci 23:127–153.

Hendry SHC, Yoshioka T. 1994. A neurochemically distinct third channel in the macaque dorsal lateral geniculate nucleus. Science 264:575–577.

Jacobs GH, Deegan JF, Neitz J, Crognale MA, Neitz M. 1993. Photopigments and color vision in the nocturnal monkey, *Aotus*. Vis Res 33: 1773–1783.

Jacobs GH, Neitz M, Neitz J, Deegan JF. 1996. Trichromatic colour vision in New World monkeys. Nature 382:156–158.

Johnson JK, Casagrande VA. 1995. Distribution of calcium-binding proteins within the parallel visual pathways of a primate (*Galago crassicaudatus*). J Comp Neurol 356:238–260.

Kaplan E, Lee BB, Shapley RM. 1990. New views of primate retinal function. In: Osborne N, Chader J, editors. Progress in retinal research, vol 9. Oxford: Pergamon. p 273–336.

Kolb H, Linberg KA, Fisher SK. 1992. Neurons of the human retina: a Golgi study. J Comp Neurol 318:147–187.

Lachica EA, Casagrande VA. 1993. The morphology of collicular and retinal axons ending on small relay (W-like) cells of the primate lateral geniculate nucleus. Vis Neurosci 10:403–418.

Livingstone MS, Hubel DH. 1984. Anatomy and physiology of a color system in the primate visual cortex. J Neurosci 4:309–356.

Martin PR, White AJR, Goodchild AK, Wilder HD, Sefton AE. 1997. Short communication: evidence that blue-on cells are part of the third geniculocortical pathway in primates. Eur J Neurosci 9:1536–1541.

Mize RR. 1999. Calbindin 28kD and parvalbumin immunoreactive neurons receive different patterns of synaptic input in the cat superior colliculus. Brain Res 843:25–35.

Peterson BB, Dacey DM. 1999. Morphology of wide-field, monostratified ganglion cells of the human retina. Vis Neurosci 16:107–120.

Peterson BB, Dacey DM. 2000. Morphology of wide-field bistratified and diffuse human retinal ganglion cells. Vis Neurosci 17:567–578.

Rodieck RW, Watanabe M. 1993. Survey of the morphology of macaque retinal ganglion cells that project to the pretectum, superior colliculus, and parvicellular laminae of the lateral geniculate nucleus. J Comp Neurol 338:289–303.

Schiller PH, Logothetis NK. 1990. The color-opponent and broad-band channels of the primate visual system. Trends Neurosci 13:392–398.

Shapley RM, Perry VH. 1986. Cat and monkey retinal ganglion cells and their visual functional roles. Trends Neurosci 9:229–235.

Shostak Y, Ding Y, Mavity-Hudson JA, Casagrande VA. 2002. Cortical synaptic arrangements of the third visual pathway in three primate species: *Macaca mulatta*, *Sciureus saimiri*, and *Aotus trivirgatus*. J Neurosci 22:2885–2893.

Solomon SG, White AJR, Martin PR. 2001. Extraclassical receptive field properties of parvocellular, magnocellular, and koniocellular cells in the primate lateral geniculate nucleus. J Neurosci 22:338–349.

Spear PD, Kim CBY, Ahmad A, Tom BW. 1996. Relationship between numbers of retinal ganglion cells and lateral geniculate neurons in the rhesus monkey. Vis Neurosci 13:199–203.

Sterling P. 1998. Retina. In: Shepherd GM, editor. The synaptic organization of the brain. New York: Oxford University Press. p 205–253.

Tigges J, Tigges M. 1987. Termination of retinofugal fibers and lamination pattern in the lateral geniculate nucleus of the gibbon. Fol Primatol 48:186–194.

Ts'o DY, Gilbert CD. 1988. The organization of chromatic and spatial interactions in the primate striate cortex. J Neurosci 8:1712–1727.

van Horn SC, Erisir A, Sherman SM. 2000. Relative distribution of synapses in the A-laminae of the lateral geniculate nucleus of the cat. J Comp Neurol 416:509–520.

Wässle H, Boycott BB. 1991. Functional architecture of the mammalian retina. Physiol Rev 71:447–480.

White AJR, Solomon SG, Martin PR. 2001. Spatial properties of koniocellular cells in the lateral geniculate nucleus of the marmost *Callithrix jacchus*. J Physiol 533:519–535.

Wilson JR. 1993. Circuitry of the dorsal lateral geniculate nucleus in the cat and monkey. Acta Anat 147:1–13.

Wilson JR, Hendrickson AE. 1981. Neuronal and synaptic structure of the dorsal lateral geniculate nucleus in normal and monocularly deprived *Macaca* monkeys. J Comp Neurol 197:517–539.

Xu X, Ichida JM, Allison JD, Boyd JD, Bonds AB, Casagrande VA. 2001. A comparison of koniocellular, magnocellular and parvocellular receptive field properties in the lateral geniculate nucleus of the owl monkey (*Aotus trivirgatus*). J Physiol 531:203–218.